Overcoming Rayleigh–Plateau instabilities: Stabilizing and destabilizing liquid-metal streams via electrochemical oxidation

Minyung Song[a], Karin Kartawira[a], Keith D. Hillaire[b], Cheng Li[a], Collin B. Eaker[a], Abolfazl Kiani[a], Karen E. Daniels[b,1], and Michael D. Dickey[a,1]

[a]Department of Chemical & Biomolecular Engineering, North Carolina State University, Raleigh, NC 27695; and [b]Department of Physics, North Carolina State University, Raleigh, NC 27695

Edited by David A. Weitz, Harvard University, Cambridge, MA, and approved June 26, 2020 (received for review April 3, 2020)

Liquids typically form droplets when exiting a nozzle. Jets—cylindrical streams of fluid—can form transiently at higher fluid velocities, yet interfacial tension rapidly drives jet breakup into droplets via the Rayleigh–Plateau instability. Liquid metal is an unlikely candidate to form stable jets since it has enormous interfacial tension and low viscosity. We report that electrochemical anodization significantly lowers the effective tension of a stream of metal, transitioning it from droplets to long (long lifetime and length) wires with 100-μm diameters without the need for high velocities. Whereas surface minimization drives Rayleigh–Plateau instabilities, these streams of metal increase in surface area when laid flat upon a surface due to the low tension. The ability to tune interfacial tension over at least three orders of magnitude using modest potential (<1 V) enables new approaches for production of metallic structures at room temperature, on-demand fluid-in-fluid structuring, and new tools for studying and controlling fluid behavior.

liquid metal | Rayleigh instabilities | EGaIn | jetting | jets

Fluids pumped from a nozzle at low flow rates form droplets to minimize interfacial energy. It is possible to transition from this dripping mode to smooth cylindrical jets by increasing the velocity of the fluid (1, 2) or by using the shear from a surrounding fluid (3). Such jets are found both in mundane streams, such as water flowing from a faucet, as well as in important applications such as industrial sprays, fuel injection systems, polymeric fibers, inkjet nozzles, and even nuclear fission (4, 5). Because the breakup of jets occurs via the Rayleigh-Plateau instability, driven by the destabilizing effects of interfacial tension, it is possible to suppress the onset of the instability by either decreasing the tension or by increasing the viscosity (6–8). Nonetheless, it has not been possible to eliminate the instability: even streams of dry granular materials —having nominally zero surface tension— can rapidly break up into clusters via the weak cohesion between the colliding particles (9).

We report that a liquid metal —eutectic gallium indium (EGaIn) (10–13)— is able to form long-lived stable jets. The term 'jets' normally implies fast moving streams, but here the velocities are low, yet still have cylindrical shapes that resemble jets. Remarkably, these cylindrical streams form despite every condition being unfavorable for jet formation: low flow rates, small diameters, and a fluid with low (water-like) viscosity and an interfacial tension significantly larger than any other fluid at room temperature. Because of these properties, liquid metals pumped from an orifice typically form droplets via the dripping mode (5, 14, 15). Droplets form even if the surface reacts with air to form a solid, native oxide skin, which opposes extrusion in a manner similar to surface tension (12). Because of liquid metals' large surface tension, jets only form at extreme ejection velocities (>1 m/s) or by using viscous sheath flow (15). In either case, the jets breakup nearly instantly (16–19); linear stability analysis predicts instabilities to occur within ∼0.1 μs for thin streams of bare metal (20) and experiments show that streams of surface oxidized metal in microfluidic shear flow break up within ∼0.1 s (15). Cylindrical structures can also form in air by shearing the metal out of a nozzle in close proximity to a substrate to which the oxide-coated metal adheres (21–23). The surface oxide stabilizes these structures against the destabilizing effects of interfacial tension, although the resulting structures are static and remain attached to the substrate. Despite these challenges, the ability to manipulate free-flowing streams of metal at room temperature is promising for forming and reconfiguring soft and stretchable conductors on demand (24, 25) as well as shaping liquids within liquids (26).

Here, we show it is possible to tune free-flowing streams of EGaIn liquid metal from the dripping regime to stable cylinders of metal in alkaline electrolyte by imposing modest electric potentials. Whereas liquid jets normally form by increasing velocity (inertia), here we utilize electrochemical oxidation to lower the effective tension (27–29). Because of the lowered tension, cylinders of metal form at a velocity (∼1 cm/s) that is orders of magnitude lower than what would normally be required to form

Significance

Liquid streams emerging from a nozzle break up rapidly into droplets due to Rayleigh–Plateau instabilities driven by surface tension. Liquid metals have enormous surface tension yet can be formed into stable cylindrical streams by applying an oxidizing potential to the metal as it is injected into an electrolyte at low velocities. The interfacial tension of a stream of liquid metal can be manipulated electrochemically in real time to produce a range of morphologies, including droplets, fine (100-μm diameter) wires, and rough shapes. The liquid wires can flow and bend without breaking over long distances. This phenomenon enables new approaches for production of metallic structures at room temperature, on-demand fluid-in-fluid structuring, and new tools for studying and controlling fluid behavior.

Author contributions: M.S., K.D.H., C.L., C.B.E., A.K., K.E.D., and M.D.D. designed research; M.S., K.K., C.L., and C.B.E. performed research; M.S. contributed new reagents/analytic tools; M.S., K.D.H., A.K., K.E.D., and M.D.D. analyzed data; M.S., K.D.H., A.K., K.E.D., and M.D.D. wrote the paper; and all authors contributed to scientific discussion and experimental design.

The authors declare no competing interest.

This article is a PNAS Direct Submission.

Data deposition: The data that support the findings of this paper are available at the Harvard Dataverse database, https://doi.org/10.7910/DVN/2MNS3G.

[1]To whom correspondence may be addressed. Email: kdaniel@ncsu.edu or mddickey@ncsu.edu.

This article contains supporting information online at https://www.pnas.org/lookup/suppl/doi:10.1073/pnas.2006122117/-/DCSupplemental.

First published July 29, 2020.

jets of liquid metal with similar diameters. When pumped from a nozzle at low flow rates (in which inertia is insignificant), gravity pulls the metal downward to form a cylindrical stream that remains stable even as it passes over obstacles. Notably, when draped onto a flat surface, such cylinders of fluid *increase* in surface area, whereas Rayleigh instabilities normally break-up cylinders of fluid into droplets to decrease the surface area. We refer to the resulting cylindrical structures as 'wires' both to distinguish this morphological regime from jets (since unlike jets, the wires are not forming at high velocity) and because of their stability, narrow diameter (100 μm), metallic conductivity, and high aspect ratio. By using electrical potential to tune the magnitude of dimensionless numbers (Bond, Weber and Froude numbers are known to capture the relative importance of forces acting on a stream), it is possible to stabilize and destabilize liquid streams, on demand and in real time, across a rich phase diagram of stream morphologies. More generally, the use of electrochemical surface reactions is a promising approach to alter the interface of liquid streams due to its simplicity, rapid response, and precise control.

Results

Fig. 1*A* depicts the experimental apparatus and Fig. 1*B* illustrates each of the morphologies as the applied electric potential ε increases (Movie S1). In the absence of ε, pumping the metal at a velocity v into 1 M NaOH (aq) produces a series of large *drops* due to the high interfacial tension γ of bare EGaIn. Applying a sufficiently positive ε to the metal oxidizes the surface and significantly lowers the effective interfacial tension γ, causing the droplet sizes to decrease (note: we use the term effective γ because the interface is not a pure fluid-fluid interface when it supports oxide species). Upon further increasing ε, we observe that the drops begin to form *connected drops* (i.e., drops that form at the nozzle and leave behind a thin 'tail' each time they fall) before finally transitioning to smooth *wires* as γ continues to decrease with potential. At still larger values of ε, the wires become unstable, forming irregular, drop-like *blobs* as the oxide layer thickens and physically disrupts the flow of the metal. Spatially-extended *tree-like wires* form only at the lowest v, where we speculate that the low shear forces provide the most favorable conditions for the oxide to adhere to the nozzle.

Fig. 1*C* shows the phase diagram of the morphological regimes of EGaIn as a function of v and ε. Each horizontal line of data points captures the observed morphologies for a potentiometer scan rate of 1 mV/s; this rate is selected to be sufficiently slow to ensure the observed morphologies are effectively at steady-state. Multiple experiments were performed to demonstrate reproducibility. The maximum velocity was limited by the leakage of liquid metal at the junction of the syringe and the needle. Technically, we were able to form wires at a lower v than reported here, however, it is excluded in Fig. 1*C* because we were not able to observe all of the morphologies at the lowest velocities. The transition boundaries are approximately the same for two different nozzle inner diameters, $d = 100$ μm and $d = 200$ μm (*SI Appendix A*, Fig. S1). The morphologies reported in Fig. 1 are identified by visual inspection, but they also each have characteristic features which can be observed in the graph of current I vs. applied potential ε, as shown in Fig. 2*A*. The morphological transitions in Fig. 1*C* from *drops* to *connected drops* and finally to *wires* all occur at ε that are independent of v (*SI Appendix A*, Fig. S2); these transitions are denoted by the vertical, black dotted boundary lines in Fig. 1*C*. This morphological dependence on ε (and lack of dependence on v) suggests that these transitions are due primarily to electrochemical reactions, rather than inertia. In the sections that follow, we discuss and analyze each of these regimes, in sequence from low to high ε.

In the *drop* regime, the interfacial tension supports the growing droplet at the nozzle, against the forces of gravity, until the droplet reaches a critical diameter, L, as in ordinary dripping. The dimensionless *Bond number* (Bo), also called the *Eötvös number* (Eo), defines this critical dimension via the ratio of gravitational forces to interfacial forces. Droplets fall from the nozzle near Bo ~1 (forces approximately equal), at which point

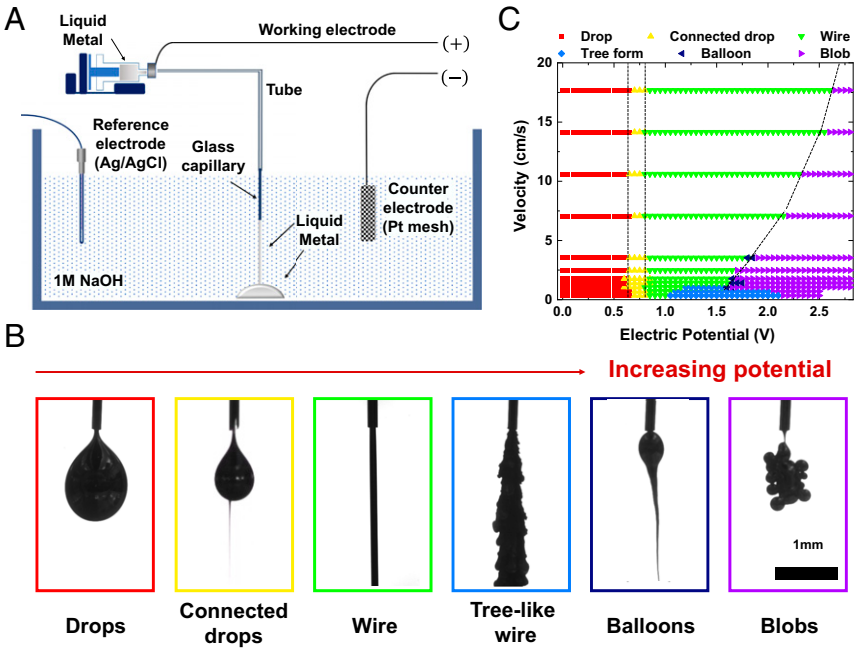

Fig. 1. (*A*) Schematic of the three-electrode system used for studying the morphology of liquid metal while varying the electric potential (ε) and velocity (v). Liquid metal, which serves as the working electrode, is pumped from a glass capillary into a bath of 1 M NaOH electrolyte containing a reference and counter electrode. (*B*) Experimental images of the liquid metal morphologies observed as a function of potential (ε) at $v = 0.35$ cm/s (flowrate: 0.1 mL/h). The nozzle diameter is $d = 100$ μm. (*C*) Phase diagram of EGaIn streams at different velocities subject to ε. The dashed lines correspond to the boundaries.

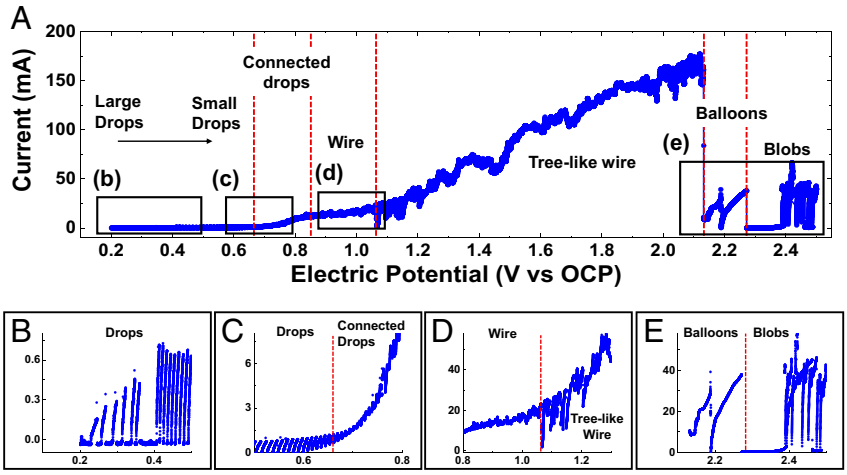

Fig. 2. (*A*) Measured current (*I*) as a function of applied electric potential (ε) of a liquid metal stream exiting a nozzle. (*B–E*) Expanded views of regions from part (*A*) to show characteristic and distinct behavior at the boundary of different regimes. The scan rate and metal velocity were 1 mV/s and v = 0.35 cm/s (flowrate: 0.1 mL/hr) respectively.

$\gamma = \Delta\rho g L^2$, where $\Delta\rho$ is the density difference between EGaIn and NaOH and g is the gravitational acceleration. The transition from larger to smaller *drops* occurs at a potential corresponding to surface oxidation, consistent with cyclic voltammetry measurements (28) and measurements of the tension of sessile drops. At this potential, there is a sharp decrease in γ and thus, decrease in the size of the droplets Fig. 3*A*. At these potentials, the oxidation is passivating (covering the metal with the thin layer that limits current), as indicated by the plateau in the current density during the life cycle of one droplet (Fig. 3 *B* and *C* and *SI Appendix A*, Fig. S3). Both γ, and thus L, continue to decrease with an increase in applied ε (Fig. 3*A*) until the morphology transitions to the *connected drops*, which corresponds with an increase in current near 0.7 V (Fig. 2*C*).

The *connected drop* regime occurs as the system transitions from droplets to wires. At $\varepsilon > 0.7$ V, the drops form a tail each time they fall from the nozzle. This tail remains connected to the metal within the nozzle and thus hangs from the next drop that grows at the nozzle. Because of the tail, it is not possible to estimate the γ in this regime using pendant drop shape analysis. These droplets with tails are different from the beads on a string that often form as threads thin by Rayleigh instabilities (31). Here, the droplets form at the nozzle, whereas Rayleigh instabilities occur on a thread of liquid downstream of the nozzle. The stability of the narrow tail suggests the tension is low and stabilized by the oxide on this portion of the surface, yet the periodic formation of droplets suggests there may be a gradient in tension (i.e., nonzero tension) as fresh metal exits the nozzle. Whereas I decreases to effectively zero each time a droplet falls, I remains finite in the *connected drop* regime because the liquid metal (working electrode) remains in contact with the solution by this tail of fluid (*cf* Fig. 2*C*). As the tail gets longer with increased ε (suggesting a further drop in tension), I increases gradually due to the surface area increase as illustrated in Fig. 2*C*.

When $\varepsilon > \sim 0.8$ V, the metal exits the nozzle as a continuous cylindrical stream, in the form of a free-falling wire. This potential is noteworthy since prior studies of sessile drops show that near 0.8 V the metal behaves as if γ is near zero (28). The transition to wires shows a lack of dependence on velocity (Fig. 1), suggesting the drop in tension is the dominant factor over the range of velocities explored. The resulting wires taper slightly over a distance of 1 cm from the nozzle and then remain constant in diameter as they fall. The diameters are similar in value to the nozzle d (~100 μm, *SI Appendix A*, Fig. S4), although the diameter increases with flow rate. The steady state wire diameter indicates that the average v of the liquid metal does not change significantly along its length and that viscous drag from the electrolyte balances against gravitational forces (32) (Discussed more in *SI Appendix A*, Fig. S5).

To rule out the possibility that the oxide forms a static cylindrical shell through which the liquid metal flows, we tracked several particles on the surface of the wires as they exited the nozzle (Fig. 4*A*). These particles moved downward with the surface, confirming that the shell is not a static tube (Fig. 4*B*). Near the nozzle, the movement of the surface particles shows the outer layer accelerates to reach a steady state profile downstream. The lack of tapering of the diameter further from the nozzle indicates the average velocity of the wire is constant (~8.8 mm/s in Fig. 4*B*), although the velocity profile is likely nonuniform within the wire.

To demonstrate that the wires are both stable and nonrigid, we moved the nozzle across several macroscopic stair steps, as shown in Fig. 4*C* and Movie S2. We observe that the lowest portion of the wire droops at a downward rate of 4 mm/s, approximately half that of the fluid velocity at the nozzle (8.8 mm/s). This suggests that the wire has a string-like behavior, since a stream of liquid would be free to fall at a faster rate dictated by the balance of gravity and viscous drag. We note that the center (lowest portion) of the drooping wire gets thicker due to gravity, suggesting the suspended metal can flow within its oxide skin without inducing an instability (Movie S2). To further demonstrate the string-like behavior, we draped a liquid metal wire across two platforms. As seen in Fig. 4*D*, liquid metal not only spanned the obstacles, but also moved upward when suddenly tugged, suggesting the oxide species on the surface provide some elastic behavior at short time scales (Movie S3). Fig. 4*E* (Movie S4) shows a wire of the liquid metal descending down ramps of alternating incline. In the absence of potential (at the end of Movie S4), the wire breaks up into droplets immediately. The metal wire remains connected throughout this complex pathway. Whereas solid-like coatings at the interface of a liquid stream can cause kinking (6), here the liquid wires undergo coiling at the bottom of the container (Movie S5) (33).

Taken together, the results of Fig. 4 shows that the oxidized interface helps stabilize the wires, yet it does not act as a completely rigid shell. Two factors likely facilitate this behavior. First, the ability to simultaneously dissolve (via NaOH) and electrochemically deposit oxide results in a dynamic surface that

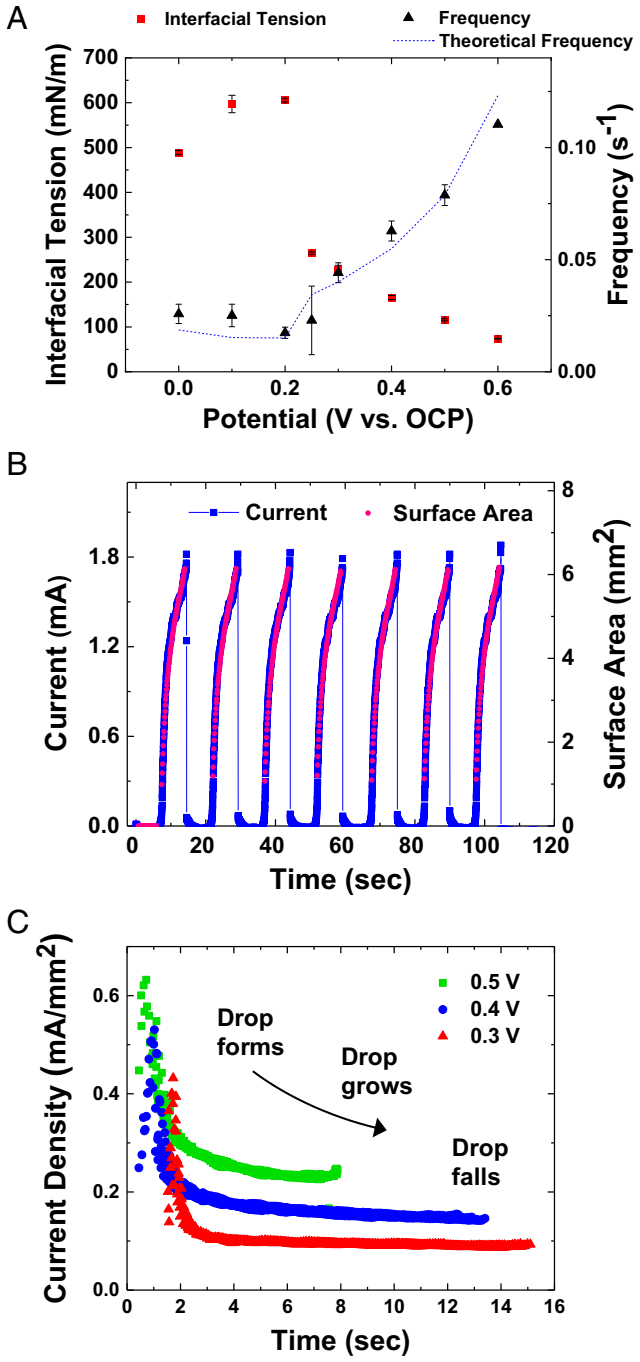

Fig. 3. (*A*) Interfacial tension γ of the liquid metal measured by drop shape analysis (left axis, solid red square) and both measured and theoretical frequency (right axis, solid black triangle and dotted line respectively) as a function of potential (ε). The theoretical frequency was calculated from Q/V_m, where V_m is the maximum drop volume. V_m was calculated by Tate's law ($\rho V_m g = \pi d\gamma$ where g is the gravitational force) (30). Error bars for γ are too small to be visible. Average droplet frequency was obtained by measuring the time Δt to form a droplet, repeated for $n = 7$ consecutive droplets. To measure the (*B*) current $I(t)$ (blue line) and surface area $A(t)$ (solid magenta round) collected at $\varepsilon = 0.5$ V. (*C*) Current density $J(t)$ for a growing drop within the *drop* regime measured by chronomamperometry. Green squares, blue circles, and red triangles represent 0.5 V, 0.4 V, 0.3 V respectively. For (*A–C*) velocity was fixed at $v = 0.35$ cm/s (flowrate: 0.4 mL/h) from a glass capillary with d of 200 μm.

allows the wire to flow despite the presence of an ultra-thin layer of oxide species. Second, prior work on sessile drops (29) suggest that at these potentials, surface oxidation can cause the surface area of the metal to increase via gravitational spreading, suggesting that the surface is capable of flowing and expanding despite the presence of oxide species. We observe a similar behavior when we drape a wire flat across a surface (Movie S6). This highlights another unique feature of this system: Unlike surfactants that must diffuse to and then assemble on surfaces (7, 34), an electrochemically-generated oxide deposits immediately in exposed regions and can be reversibly removed. Yet unlike solid species, the surface does not kink when bent and expands in surface area when the metal stream stops flowing.

Notably, at larger potentials ($\sim 1\ \text{V} \leq \varepsilon \leq \sim 2\ \text{V}$), the oxide thickens and disrupts the metal to flow freely, resulting in the irregular shapes shown in Fig. 1*B*: *balloons*, *blobs*, and *tree-like wires* (the ε values at which this occurs depends on v, see Fig. 1 and *SI Appendix A*, Fig. S1). All of these states have a visibly matte surface, indicative of a thick, rough oxide layer. The resulting morphologies, and their nuanced differences that result from the obstructed flow, are discussed in the *SI Appendix A*, Fig. S6). The thick oxide layer results in a sudden drop of current (Fig. 2*A*), which is consistent with a physical surface layer that obstructs current (*SI Appendix A*, Fig. S7). Notably, a thick oxide crust also forms in the droplet regime when NaOH is replaced with NaCl or other pH neutral electrolytes.

Discussion

The most unexpected aspect of these results is the formation of wires considering that (1) the bare metal has the largest tension of any liquid at room temperature (>500 mN/m at $\varepsilon = 0$) (2), conventional jets with sub-mm diameters form only at velocities that are orders of magnitude larger than those used here, and (3) jets with similar bulk viscosity and ultralow tension breakup rapidly. For example, a water jet with a similar diameter and bulk viscosity only forms in oil when exiting a nozzle at ~33 cm/s, with a lifetime of ~0.07 s (35).

Here, the ability to use potential to tune the interfacial tension over an enormous range controls the flow morphology from droplets to wires. Remarkably, at Bo ~ 1, γ would need to be less than 1 mN/m to produce droplets with diameters of $L = d$ via gravitational forces. Yet wires form rather than small droplets, suggesting the tension is even lower.

The ability to control tension makes it possible to tune dimensionless numbers over large ranges. For example, the *Weber number*, We $\left(= \frac{\Delta\rho v^2 d}{\gamma}\right)$ varies from 3×10^{-8} (for drops) to $>6 \times 10^{-1}$ (for wires, assuming an upper value of 1 mN/m) over a range of only 0–0.8 V. Thus, despite the low velocity of the wires, inertial forces cannot be completely neglected when compared to the extraordinarily low interfacial tension at 0.8 V. Yet, there is no evidence to suggest inertia plays an important role in wire formation. For example, the wires remain stable even when the velocity is slowed—either by changing velocity or by drooping them over surfaces (Fig. 4). Furthermore, the wires fall downward immediately upon exiting a horizontally oriented nozzle, suggesting gravity is more important than inertia (Fr varies from 0.1 to 6 in the wire regime). Dimensionless numbers are discussed more in the *SI Appendix B*.

The longest wire we created was equal to the tallest transparent container in our laboratory, 64 cm (Fig. 4*F* and Movie S7). Remarkably, wires this long have a height: diameter aspect ratio of >6400 which is at least two orders of magnitude higher similar streams of water (36). In principle, longer wires are likely possible. During the ~18 s it takes to fall 64 cm, the metal has the opportunity to undergo Rayleigh-Plateau instabilities. The

ENGINEERING

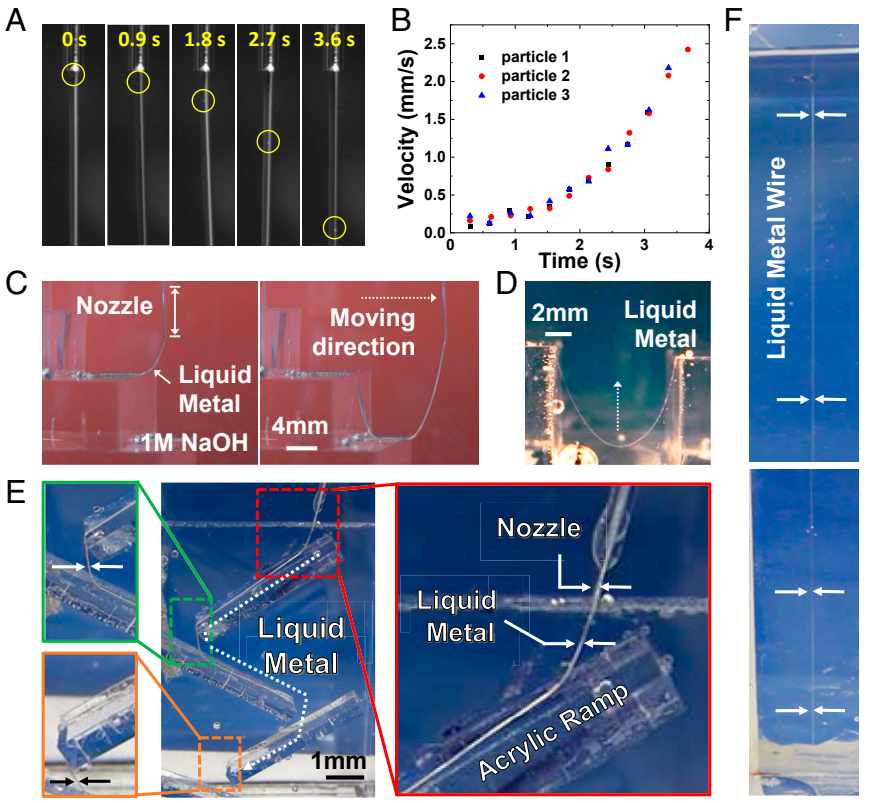

Fig. 4. (*A*) Sequential images of encircled particles moving downward along the surface of a wire exiting the nozzle prove that the oxide does not form a static shell. (*B*) Velocity of tracer particles on the surface of the EGaIn wire as a function of time, with $t = 0$ representing the particle movement from the nozzle tip. The measurement presented a SE of 20 μm. (*C–E*) A photograph of liquid metal wires in the *wire* regime. The liquid metal wire maintains its shape (*C*) as the glass capillary nozzle moves across steps (Movie S2), (*D*) across two platforms (Movie S3) and (*E*) down alternating ramps (Movie S4). (*F*) The wire did not undergo any instabilities as it flows into a 64 cm tall container (Movie S7). The wire is so long that it did not fit into a single picture frame. The graph and photographs are taken at 1 V and 0.8 V respectively with an average velocity $v = 8.8$ mm/s (flowrate: 1 mL/h) and $d = 200$ μm.

scaling relationship $\tau = \left(\frac{\Delta\rho d^3}{8\gamma}\right)^{\frac{1}{2}}$ predicts the time τ necessary for an inviscid cylindrical stream to undergo such an instability as a function of diameter, tension, and density difference between the liquid metal and the electrolyte (37, 38). Since the EGaIn wires are not observed to undergo such an instability, we find the upper limit on γ to be 1.5×10^{-8} mN/m based on this scaling (this value increases to 2.2×10^{-5} mN/m if the viscosity of the surrounding medium is accounted for, see *SI Appendix B*). However, prior studies show that even jets with extremely low γ are not stable (9). Therefore, it is likely that the oxide species facilitate wire formation. Perhaps most importantly, when the wire is draped across a surface and the metal ceases to flow as a stream, the cylindrical shape *increases* in surface area rather than decrease (Fig. 4*C* and Movie S6), which shows that the surface can flow (i.e., it is not a rigid shell) and in doing so, increases its surface area rather than decrease – as associated with Rayleigh-Plateau instabilities. Using the wire diameter as the capillary length, the effective tension must be <0.1 mN/m since such a structure increases its area by flattening in response to gravity when laid along a horizontal surface. This value is consistent with our prior estimates (29).

As a point of contrast, we note that pumping liquid metal from a nozzle into air does not result in wires, but rather forms droplets with a solid native oxide shell; thus, surface oxidation itself is not sufficient to form wires. Electrochemical oxidation causes sessile droplets of metal to flow and expand in surface area under the conditions used here to achieve wires (1 M NaOH, 0.8 V) (28, 29). This is noteworthy because liquids normally adopt shapes that minimize surface energy, including the droplets that form during Rayleigh instabilities. The presence of these oxide species also appears to provide stabilizing effects in the radial direction, as illustrated by the wispy tails that hang from the ends of the metal in the *connected drop* and *balloon* regimes (Movie S8) (note that these two regimes have similar morphology, but they differ from one another by the current profile). While we expect that a dense liquid emerging from a nozzle with near-zero γ should fall at a rate that is retarded only by viscous drag from the surrounding electrolyte, these tails neither fall freely, nor recoil due to γ. This behavior is consistent with the presence of oxide species on the surface that both lowers the effective γ and helps stabilize these structures.

The measurements of I (Fig. 2) is an important clue for understanding the formation of wires. At low potentials, the surface oxide is thin, yet passivating. The formation of wires associates with the dramatic rise in current by a factor of 20, as expected for passive oxide breakdown, which drives current through the oxide layer and creates compressive interfacial stress that helps offset the tension of the metal. At larger potentials, the current drops to near zero, and the wire regime abruptly ends due to a thickening oxide that both obstructs the flow and ceases to cause compressive surface stresses necessary for the metal to form wires. At these high potentials, the metal does not grow as a smooth drop, but rather as multiple hemispherical protrusions (Movie S9).

This paper shows the effect of an applied electric potential, ε, on a stream of liquid metal exiting from a small nozzle (with an opening similar to the diameter of a human hair) into 1 M NaOH. The resulting oxidative process significantly affects the morphology of the falling metal stream. Although we distinguish six different morphologies in this paper, these can be classified into three broad classes: surfaces with no oxide, some oxide, and thick oxide. In the absence of oxide, the metal forms large drops. Upon oxide formation, the droplets get smaller and continue to decrease in size (consistent with the effective interfacial tension, γ, dropping) until the metal eventually forms cylindrical wires. The formation of wires suggests the effective γ is near zero. In addition to lowering the tension, the dynamic oxide coating gives the wires string-like behavior over short time scales, yet the wires retain the ability to flow. At higher ε, the observation of a much smaller current suggests a thick oxide, adhered to the nozzle and visually apparent as a matte surface, which disrupts the flow and results in highly-structured morphologies.

These results are interesting because liquid metals have low viscosity and enormous γ, making them ideal candidates for forming dripping or Rayleigh-Plateau instabilities. Yet they form unexpectedly wires and other unusual shapes via application of modest electric potential. The use of electric potential allows for rapid, reversible and huge changes in effective γ, from >500 mN/m to near zero that is not possible with surfactants (39). The results suggest it is possible to form a wire using <1 V with constant (low) velocity whereas the conventional way of forming jet is by significantly increasing the velocity. The most useful and remarkable implication is the possibility to overcome Rayleigh-Plateau instabilities using a fluid that is the least likely candidate to do so based on its viscosity, dimensions (similar to a long human hair), and bare metal tension. This ability to create continuous sub-mm diameter wires of liquid metal may offer new ways of creating soft, stretchable electronic devices at room temperature, although future work is needed to find ways to encapsulate the metal so that the wires may be collected for later use.

Materials and Methods

Experimental Procedures. A syringe pump injected EGaIn into an electrolyte bath via a tube connected to a glass capillary (we refer to this as the nozzle throughout). Most of the experiments were conducted by pumping between 0.1 mL/h and 5 mL/h through $d = 100$ μm inner diameter and 170 μm outer diameter glass capillaries from a height of ~3.5 cm above the bottom of the electrolytic cell, unless stated otherwise. Velocity v was calculated by the equation: $v = \frac{Q}{A}$, where Q is the flowrate (controlled by a syringe pump) and A is the cross-sectional area of the nozzle opening.

The electrolytic cell (5 cm × 7.5 cm × 5 cm) contains three electrodes: EGaIn serves as the working electrode, platinum gauze (25 mm × 25 mm × 52 mm mesh) as the counter electrode and saturated Ag/AgCl electrode as the reference electrode. We varied the electric potential ε with a potentiostat (Gamry, Reference 600) and measured the resulting current I. The open circuit potential (OCP) of EGaIn is −1.50 V ± 0.025 V measured with respect to the reference electrode. Thus, all of the reported potential values in this paper are shifted relative to this OCP by adding 1.5 V to the measured value (i.e., ε = 0 at the OCP).

To confirm that the scan rate was sufficiently slow for the surface oxidation and dissolution reactions to reach steady-state at any given potential, we measured the interfacial tension of a sessile droplet while scanning the potential at 1 mV/s. We compared these values to interfacial tension measurements at constant potential. The tension measurements agreed, suggesting steady-state conditions are reached at 1 mV/s. Additionally, we were able to produce a wire using chronoamperometry (a technique that uses fixed voltage) by selecting potential within the 'wire' region of the phase diagram.

Interfacial Tension and the Drop Frequency Measurement. To quantify both the γ and the drop frequency, we used a camera to record images and measure γ with a goniometer (FTA32 software, First Ten Angstroms Company, USA). We note that goniometer uses drop shape analysis that assumes the shape of the drop is at equilibrium. Since the droplets here are growing as a function of Q, the γ values are approximate, but nevertheless show trends consistent with measurements on static droplets (*SI Appendix A*, Fig. S8) (28).

Data Availability. The data that support the findings of this paper are available at the Harvard Dataverse database, https://doi.org/10.7910/DVN/2MNS3G.

ACKNOWLEDGMENTS. We are grateful for support from the NSF under Grants CBET-1510772 and DMR-160897. We acknowledge Prof. Milad Abolhasani for helpful discussions about fluid transport.

1. M. Etzold, A. Deswal, L. Chen, F. Durst, Break-up length of liquid jets produced by short nozzles. *Int. J. Multiph. Flow* **99**, 397–407 (2018).
2. C. Clanet, J. C. Lasheras, Transition from dripping to jetting. *J. Fluid Mech.* **383**, 307–326 (1999).
3. A. S. Utada, A. Fernandez-Nieves, H. A. Stone, D. A. Weitz, Dripping to jetting transitions in coflowing liquid streams. *Phys. Rev. Lett.* **99**, 94502 (2007).
4. B. Derby, Inkjet printing of functional and structural materials: Fluid property requirements, feature stability, and resolution. *Annu. Rev. Mater. Res.* **40**, 395–414 (2010).
5. J. Eggers, E. Villermaux, Physics of liquid jets. *Rep. Prog. Phys.* **71**, 36601 (2008).
6. Z. Niroobakhsh, J. A. LaNasa, A. Belmonte, R. J. Hickey, Rapid stabilization of immiscible fluids using nanostructured interfaces via surfactant association. *Phys. Rev. Lett.* **122**, 178003 (2019).
7. A. Alhushaybari, J. Uddin, Absolute instability of free-falling viscoelastic liquid jets with surfactants. *Phys. Fluids* **32**, 13102 (2020).
8. A. Javadi, J. Eggers, D. Bonn, M. Habibi, N. M. Ribe, Delayed capillary breakup of falling viscous jets. *Phys. Rev. Lett.* **110**, 144501 (2013).
9. J. R. Royer *et al*., High-speed tracking of rupture and clustering in freely falling granular streams. *Nature* **459**, 1110–1113 (2009).
10. S. J. French, D. J. Saunders, G. W. Ingle, The system gallium-indium. *J. Phys. Chem.* **42**, 265–274 (2002).
11. J.-H. Kim, S. Kim, J.-H. So, K. Kim, H.-J. Koo, Cytotoxicity of gallium–indium liquid metal in aqueous environment. *ACS Appl. Mater. Interfaces* **10**, 17448–17454 (2018).
12. M. D. Dickey *et al*., Eutectic gallium-indium (EGaIn): A liquid metal alloy for the formation of stable structures in microchannels at room temperature. *Adv. Funct. Mater.* **18**, 1097–1104 (2008).
13. A. R. Jacob, D. P. Parekh, M. D. Dickey, L. C. Hsiao, Interfacial rheology of gallium-based liquid metals. *Langmuir* **35**, 11774–11783 (2019).
14. S. P. Lin, R. D. Reitz, Drop and spray formation from a liquid jet. *Annu. Rev. Fluid Mech.* **30**, 85–105 (1998).
15. S.-Y. Tang *et al*., Liquid-metal microdroplets formed dynamically with electrical control of size and rate. *Adv. Mater.* **28**, 604–609 (2016).
16. D. B. Wallace, Capillary instability of a jet of liquid metal. *J. Fluids Eng.* **115**, 529–532 (1993).
17. W.-H. Lai, C.-C. Chen, Oxidation effect on the monosized droplets generation of the liquid metal jet. *J. Fluids Eng.* **125**, 595–596 (2003).
18. J. Eggers, Nonlinear dynamics and breakup of free-surface flows. *Rev. Mod. Phys.* **69**, 865–930 (1997).
19. I. Cohen, M. P. Brenner, J. Eggers, S. R. Nagel, Two fluid drop snap-off problem: Experiments and theory. *Phys. Rev. Lett.* **83**, 1147–1150 (1999).
20. W. van Hoeve *et al*., Breakup of diminutive Rayleigh jets. *Phys. Fluids* **22**, 122003 (2010).
21. C. Ladd, J.-H. So, J. Muth, M. D. Dickey, 3D printing of free standing liquid metal microstructures. *Adv. Mater.* **25**, 5081–5085 (2013).
22. J. W. Boley, E. L. White, G. T.-C. Chiu, R. K. Kramer, Direct writing of gallium-indium alloy for stretchable electronics. *Adv. Funct. Mater.* **24**, 3501–3507 (2014).
23. G. Li, X. Wu, D. Lee, An oxidized liquid metal-based microfluidic platform for tunable electronic device applications. *Lab on a Chip* **15**, 766–775 (2015).
24. I. D. Joshipura, H. R. Ayers, C. Majidi, M. D. Dickey, Methods to pattern liquid metals. *J. Mater. Chem. C* **3**, 3834–3841 (2015).
25. T. Hutter, W.-A. C. Bauer, S. R. Elliott, W. T. S. Huck, formation of spherical and non-spherical eutectic gallium-indium liquid-metal microdroplets in microfluidic channels at room temperature. *Adv. Funct. Mater.* **22**, 2624–2631 (2012).
26. J. Forth *et al*., Reconfigurable printed liquids. *Adv. Mater.* **30**, e1707603 (2018).

27. C. B. Eaker, M. R. Khan, M. D. Dickey, A method to manipulate surface tension of a liquid metal via surface oxidation and reduction. *J. Vis. Exp.* **26**, e53567 (2016).
28. M. R. Khan, C. B. Eaker, E. F. Bowden, M. D. Dickey, Giant and switchable surface activity of liquid metal via surface oxidation. *Proc. Natl. Acad. Sci. U.S.A.* **111**, 14047–14051 (2014).
29. C. B. Eaker, D. C. Hight, J. D. O'Regan, M. D. Dickey, K. E. Daniels, Oxidation-mediated fingering in liquid metals. *Phys. Rev. Lett.* **119**, 174502 (2017).
30. B.-B. Lee, P. Ravindra, E.-S. Chan, A critical review: Surface and interfacial tension measurement by the drop weight method. *Chem. Eng. Commun.* **195**, 889–924 (2008).
31. C. Clasen, J. Eggers, M. A. Fontelos, J. Li, G. H. McKinley, The beads-on-string structure of viscoelastic threads. *J. Fluid Mech.* **556**, 283–308 (2006).
32. N. M. Ribe, Coiling of viscous jets. *Proc. R. Soc. A* **460**, 3223–3239 (2004).
33. N. M. Ribe, M. Habibi, D. Bonn, Liquid rope coiling. *Annu. Rev. Fluid Mech.* **44**, 249–266 (2012).
34. O. Raccurt, J. Berthier, P. Clementz, M. Borella, M. Plissonnier, On the influence of surfactants in electrowetting systems. *J. Micromech. Microeng.* **17**, 2217–2223 (2007).
35. I. L. Omocea, C. Patrascu, M. Turcanu, C. Balan, Breakup of liquid jets. *Energy Procedia* **85**, 383–389 (2016).
36. B. Ambravaneswaran, H. J. Subramani, S. D. Phillips, O. A. Basaran, Dripping-jetting transitions in a dripping faucet. *Phys. Rev. Lett.* **93**, 34501 (2004).
37. T. Nguyen-Dang *et al*., Controlled sub-micrometer hierarchical textures engineered in polymeric fibers and microchannels via thermal drawing. *Adv. Funct. Mater.* **27**, 1605935 (2017).
38. W. Yan *et al*., Advanced multimaterial electronic and optoelectronic fibers and textiles. *Adv. Mater.* **31**, e1802348 (2019).
39. F. Yun *et al*., Voltage-induced penetration effect in liquid metals at room temperature. *Natl. Sci. Rev.* **7**, 366 (2020).